Journal of Computational Acoustics, Vol. 5, No. 3 (1997) 317–336

NUMERICAL STUDY OF NOISE FROM ISOTROPIC TURBULENCE

A. WITKOWSKA and D. JUVÉ
Laboratoire de Mécanique des Fluides et d'Acoustique, UMR CNRS 5509,
Ecole Centrale de Lyon, BP 163, 69 131 Ecully Cedex, France

J. G. BRASSEUR
Department of Mechanical Engineering,
Pennsylvania State University, PA 16802, USA

Received 15 January 1996
Revised 1 October 1996

A numerical study of sound radiation by isotropic turbulence is carried out by combining turbulence simulation with Lighthill's acoustic analogy. In the first study we analyze sound generation by decaying isotropic turbulence obtained both with 64^3 Direct Numerical Simulation (DNS) and 16^3 Large Eddy Simulation (LES). Both simulations lead to similar results for acoustic power, in agreement with the numerical results of Sarkar and Hussaini, but slightly different from theoretical predictions of Proudman and Lilley. In the second study we analyze sound generation by forced stationary turbulence, simulated with 128^3 DNS using a forcing scheme which preserves turbulence structure. The acoustic power computed from the stationary turbulence is in good agreement with results obtained for decaying isotropic turbulence. The acoustic spectrum shows that the characteristic frequency of the generated sound is approximately four times the inverse eddy turnover time. The contributions of different turbulence scales to the generated noise are computed separately from filtered velocity fields. For the low Reynolds number turbulence analyzed, the scales which most contribute to noise generation are 2–3 times smaller than the energy-containing scales and lie between the energy and dissipation-rate spectral peaks.

1. Introduction

In 1952 Lighthill[1] published his "acoustic analogy" as a first attempt to predict the noise generated by turbulence and the theory became the starting point for modern aeroacoustics. His most fundamental contribution was to show that the nonlinear velocity fluctuations in a turbulent flow may be considered as quadrupolar sources of noise. The acoustic pressure in the far field can then be explicitly written as a spatial integral over instantaneous velocity derivative fluctuations.

Until recently, it was not possible to either measure or simulate the instantaneous velocity field. Consequently, Lighthill's theory was applied primarily to predict the mean features of the generated noise from the mean features of the turbulent field by modeling the source term. In 1952 Proudman[2] proposed a model for noise generation by isotropic turbulence, which has recently been revisited by Lilley.[3]

Advances in numerical methods and computer technology now make the full simulation of turbulent flows possible. Currently, one might consider three approaches to numerically compute the noise generated by turbulence:

- The "direct" method in which full compressible Navier–Stokes equations are solved both for the turbulence and the surrounding medium at rest. The acoustic pressure is thus obtained directly, without the use of any analogy. However, the computational effort is large and simulations are limited, at present, to only the largest scale motions in relatively simple geometries. Examples include the two-dimensional shear layer,[4] and the axisymmetric jet.[5]
- The "stochastic" method in which only mean turbulence variables are calculated using turbulence models. The mean characteristics of the generated sound are then obtained using Lighthill's analogy with models for the source term. This method can be applied to relatively complex flows and has been used, for example, to predict noise generation from subsonic and supersonic jets.[6,7] However, the models for source terms require strong hypotheses limiting the validity of the method.
- In the "hybrid" method the three-dimensional, time-dependent incompressible Navier–Stokes equations are solved and the instantaneous acoustic pressure is computed from the instantaneous velocity field using Lighthill's analogy. This method can be applied to more complex flows than the "direct" method while still providing the instantaneous acoustic pressure in far field. It has been applied to decaying three-dimensional isotropic turbulence by Béchara[6] and Sarkar and Hussaini.[8]

In the present work the hybrid approach is used to study noise generation by a three-dimensional isotropic turbulence. We apply both Direct Numerical Simulation and Large Eddy Simulation to compute the *decaying isotropic turbulence*. More importantly, we develop forced DNS to obtain *stationary isotropic turbulence* with realistic structure both in the dissipation scales and in the integral scales. With stationary turbulence we perform a proper frequency analysis of the acoustic pressure and study the relative contributions of different turbulence scales to turbulence generated sound.

We begin in Sec. 2 by summarizing Lighthill's theory and discussing some important issues surrounding the proper form of the analogy for applications to an excised box of turbulence. In the third section we analyze sound generation by *decaying isotropic turbulence*, computed using Direct Numerical Simulation and Large Eddy Simulation. We compare the predicted acoustic power with the theories of Proudman and Lilley. However, rapid decay of the turbulence does not allow for proper frequency analysis. Consequently, in Sec. 4, we analyze sound generation by *stationary isotropic turbulence*, computed with forced high resolution Direct Numerical Simulation. Instantaneous acoustic pressure, acoustic power and acoustic spectrum are presented and compared with the stochastic models. We end by analyzing the relative contributions of different turbulence scales to the noise by computing the acoustic power from spectrally filtered velocity.

2. Application of Lighthill's Acoustic Analogy to an Excised Volume of Turbulence

Lighthill[1] posed the problem of estimating the sound radiated by a finite region of turbulence surrounded by a fluid at rest. His fundamental idea was to restructure the Navier–Stokes equations into a non-homogeneous wave equation:

$$\frac{\partial^2 \rho}{\partial t^2} - c_0^2 \frac{\partial^2 \rho}{\partial y_j^2} = \frac{\partial^2 T_{ij}}{\partial y_i \partial y_j}\,, \tag{2.1}$$

where ρ is the density of the fluid, c_0 the speed of sound in the external medium (assumed uniform) and $T_{ij} = \rho u_i u_j + (p - c_0^2 \rho)\delta_{ij} + \tau_{ij}$ is Lighthill's stress tensor. Here p is the pressure and τ_{ij} is the viscous stress tensor, negligible when the Reynolds number of the flow is sufficiently high and generally ignored in acoustics computations.

If the turbulent Mach number is small (so $\rho \sim$ constant $= \rho_0$) and the pressure perturbations are isentropic (so $p = c_0^2 \rho$) Lighthill's tensor reduces to $\rho_0 u_i u_j$.[9] The right-hand side of Eq. (2.1) is the acoustic source, indicating that sound is generated by gradients of products of turbulent velocity fluctuations. The homogeneous wave operator on the left-hand side of (2.1) describes the propagation of sound from the turbulence sources through the external fluid.

The acoustic pressure predicted by Lighthill's equation for a fluid at rest external to the noise sources confined to a volume V is

$$p_a(\mathbf{x}, t) = p(\mathbf{x}, t) - p_0 = \frac{\rho_0}{4\pi} \int_V \left[\frac{\partial^2 u_i u_j}{\partial y_i \partial y_j}\right] \frac{1}{\xi} dV(\mathbf{y})\,, \tag{2.2}$$

where p_0 is the mean pressure in the fluid at rest, $\boldsymbol{\xi} = \mathbf{x} - \mathbf{y}$ and expressions inside the square brackets are evaluated at the retarded time $t - \xi/c_0$.

If the point $\mathbf{x}$ is chosen sufficiently far from the volume of turbulence that both $x \gg D$ and $x \gg \lambda$ (where $D \sim V^{1/3}$ and λ is the wavelength of the generated sound), Eq. (2.2) reduces to:

$$p_a(\mathbf{x}, t) = \frac{\rho_0}{4\pi c_0^2} \frac{1}{x} \int_V \left[\frac{\partial^2 u_x^2}{\partial t^2}\right] dV\,, \tag{2.3}$$

where u_x is the velocity component in the direction of $\mathbf{x}$. If, in addition, the turbulence domain is compact ($\lambda \ll D$), the retarded time difference can be ignored.

It is important to recognize that these solutions were established by Lighthill assuming a finite volume of turbulence surrounded by quiescent fluid. We have shown[10] that between forms (2.2) and (2.3) above, only expression (2.3) is appropriate to compute the noise generated by a subdomain of turbulence excised from a larger region of turbulent flow. In fact, if the entire disturbances region is not included, expression (2.2) is dominated by the flux of mass and momentum across the integration boundaries, where the volume V cuts through turbulence. These flux terms arise from the presence of spatial derivatives in (2.2) which transform to non-physical surface integrals by Gauss's theorem, leading to large overestimations of acoustic power (by as much as 50 dB).

For similar reasons, expressions of the acoustic pressure containing vorticity established by Powell,[11] Hardin[12] and Möhring[13] cannot be applied to an excised volume of turbulence. As a spatial derivative of velocity, vorticity introduces additional non-physical terms due to the flux across boundaries which produce overestimations of the generated noise (approximately 20 dB with Powell's formulation).

In conclusion, although Lighthill's analogy provides a powerful tool for computing the noise generated by turbulence, care must be taken when Lighthill's analogy is applied to excised volumes of turbulence with boundaries which cut through turbulence fluctuations.

3. Sound Generation by Decaying Isotropic Turbulence

In the absence of production both the turbulence and the acoustic pressure decays with time, making it difficult to analyze the frequency of the generated sound. Hence, the primary aim in this section is to compare computed acoustic power using DNS and LES with the theories of Proudman[2] and Lilley.[3]

3.1. *Turbulence simulations*

To simulate decaying isotropic turbulence we applied both Direct Numerical Simulation and Large Eddy Simulation, using standard pseudo-spectral algorithms for the incompressible Navier–Stokes equations in a cube with periodic boundary conditions. The solenoidal velocity components were initialized with Gaussian random numbers conforming to a chosen energy spectrum, with some rough physical characteristics.

Because DNS resolves all turbulence scales between the box-size (D) and the size of the mesh (Δ), the Reynolds number is necessarily low. For the simulation we used a 64^3 mesh with a Reynolds number based on longitudinal Taylor microscale R_λ of 25 at the beginning of the simulation. The initial turbulent energy spectrum is shown in Fig. 1. The turbulence loses memory of its initial conditions and approaches experimental grid turbulence in roughly one initial eddy turnover time τ_{L_0} (the longitudinal integral length scale L divided by a component rms velocity u').

In LES the influence of subgrid scales (scales smaller than Δ) is modeled. We applied the model by Chollet and Lesieur,[14] where a scale-dependent turbulent viscosity $\nu_T(k)$ is added to the molecular viscosity ν in the resolved-scale equations. Because only larger scales are simulated, LES can produce higher effective Reynolds numbers with lower spatial resolution than DNS. We used a 16^3 mesh with the initial Reynolds number R_λ equal to 360. The initial energy spectrum and the wavenumber k_c separating the resolved scales from subgrid scales are shown in Fig. 2.

The principal variables for the two simulations are given in Table 1. Details concerning the simulations can be found in Witkowska.[15]

3.2. *Acoustics computations*

As pointed out in Sec. 2, because the simulated turbulence is within a periodic subvolume of a theoretically unbounded flow, only expression (2.3) is appropriate to compute the acoustic

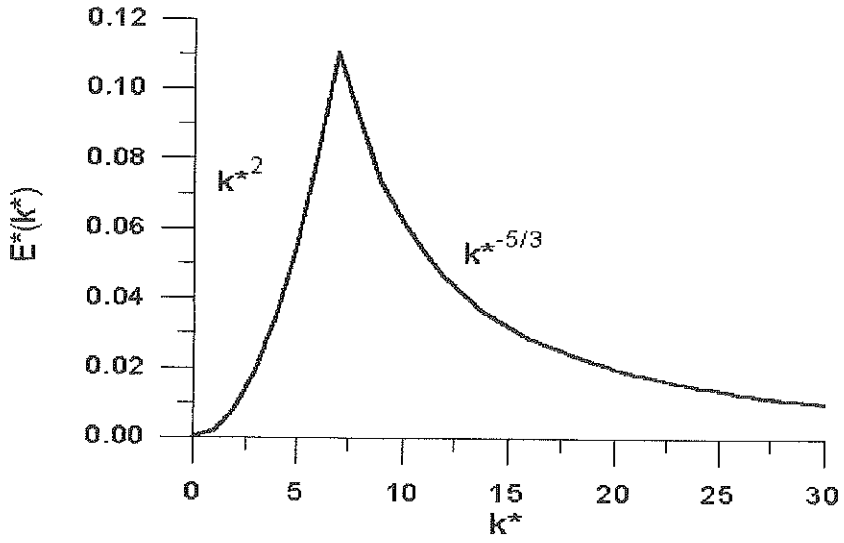

Fig. 1. Initial energy spectrum for decaying DNS ($k^* = k/\frac{2\pi}{D}$, $E^*(k^*) = E(k^*)/\int_0^\infty E(k^*)dk^*$).

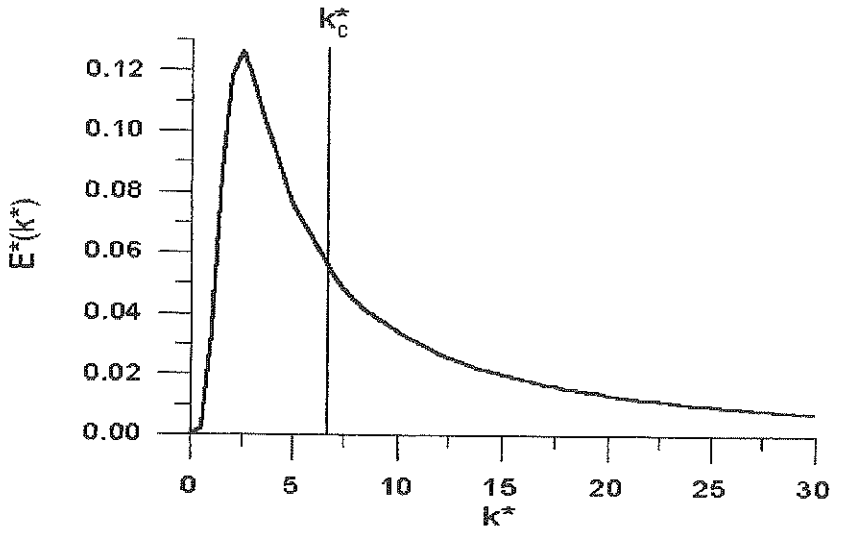

Fig. 2. Initial energy spectrum for decaying LES.

pressure. In the computations presented in this paper we took into account time delay in the Eq. (2.3), although it turns out that in this case the effect of time delay is minimal.

The acoustic pressure is computed at a point $\mathbf{x}$ situated on a line passing through the center of the cube and perpendicular to one of its sides. The point $\mathbf{x}$ is chosen sufficiently far from the turbulence volume to insure the far field condition ($x = 20D$ in the DNS and $200D$ in the LES). With the chosen time step (cf. Table 1) the time delay difference between

Table 1. The principal variables for the simulations. The first two columns give initial conditions, Δt is the time step used in the simulation, η is the Kolmogorov length scale, $k_{\max}$ is the highest resolved wavenumber after dealiazing, $M = u'/c_0$ is the turbulence Mach number.

Variable	Decaying LES	Decaying DNS	Stationary DNS
N	16^3	64^3	128^3
$R_\lambda = \frac{u'\lambda}{\nu}$	360	25	20
M	0.014	0.009	0.010
Δt	Δ/c_0	$2\Delta/c_0$	$4\Delta/c_0$
D/L	7.1	23.2	14.3
$k_{\max}$	6.3	30.5	60.3
$k_{\max}\eta$	—	0.6	1.6
Δ/η	—	10	2

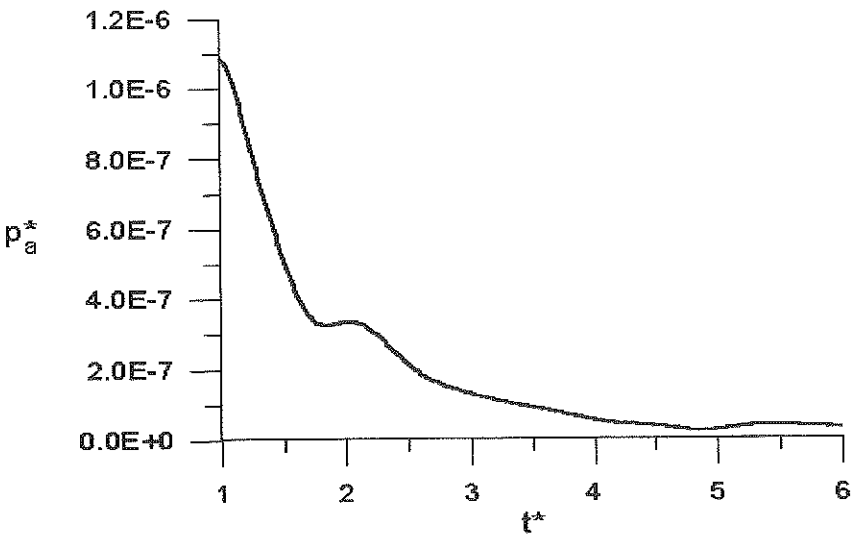

Fig. 3. Acoustic pressure calculated from a typical decaying LES ($p_a^* = p_a/(\rho_0 u_0'^2)$, $t^* = tu_0'/L_0$).

those planes perpendicular to the direction of x is taken into account (every plane for the LES, every other plane for the decaying DNS, and every fourth plane for the stationary DNS). The computations were carried out over 50 independent realizations of the initial velocity field for the LES and 10 independent realizations for the DNS.

In Figs. 3 and 4 we showed typical realizations of acoustic pressure variations with time from the LES and DNS computations. In all plots acoustic pressure is nondimensionalized by $\rho_0 u_0^2$ and time by the initial large eddy time scale τ_{L_0}. Note that acoustic pressure decreases rapidly with time due to the decaying nature of the turbulence.

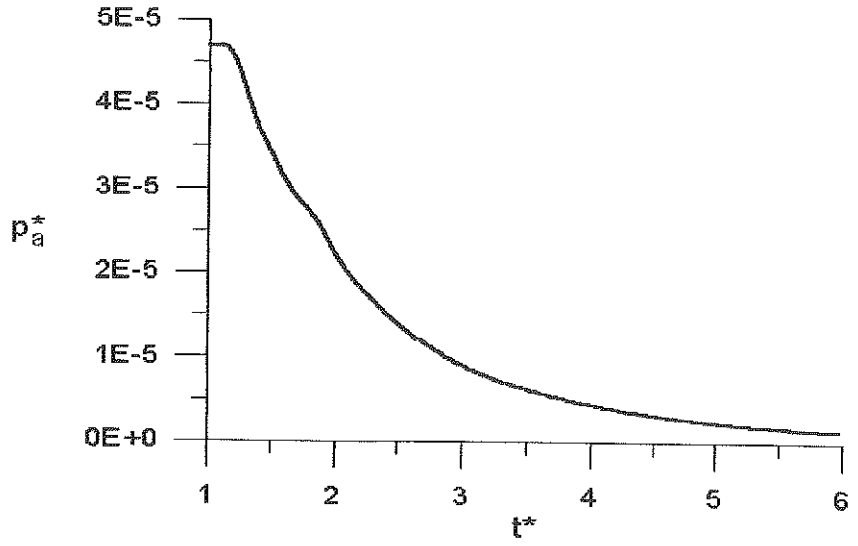

Fig. 4. Acoustic pressure calculated from a typical decaying DNS ($p_a^* = p_a/(\rho_0 u_0'^2)$, $t^* = tu_0'/L_0$).

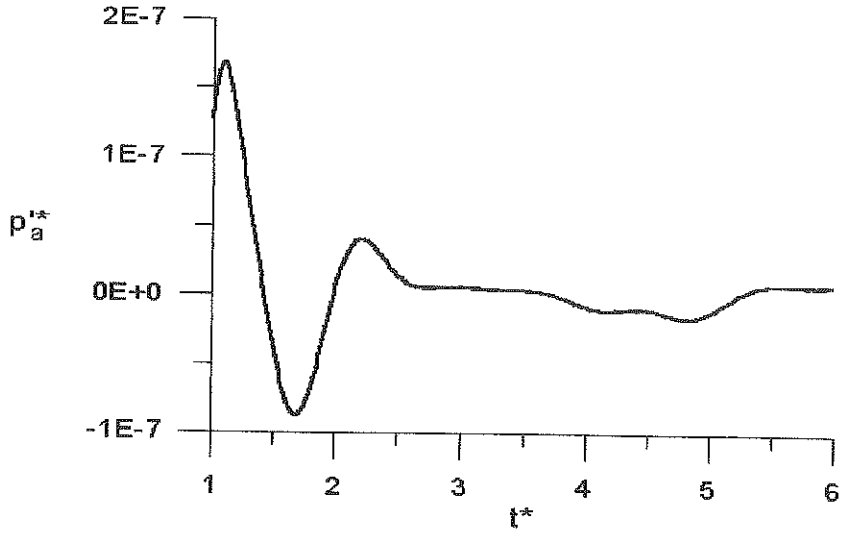

Fig. 5. Fluctuating acoustic pressure calculated from the decaying LES of Fig. 3 ($p_a'^* = p_a'/(\rho_0 u_0'^2)$).

In Figs. 5 and 6 we plot fluctuating acoustic pressure p_a' for the same realizations as Figs. 3 and 4, where

$$p_a' = p_a - \langle p_a \rangle \tag{3.4}$$

and $\langle p_a \rangle$ is the ensemble average acoustic pressure evaluated over the different realizations. Figures 5 and 6 show that the fluctuating acoustic pressure is strongly nonstationary, making it difficult to analyze the frequency of the generated sound. To the extent that a frequency

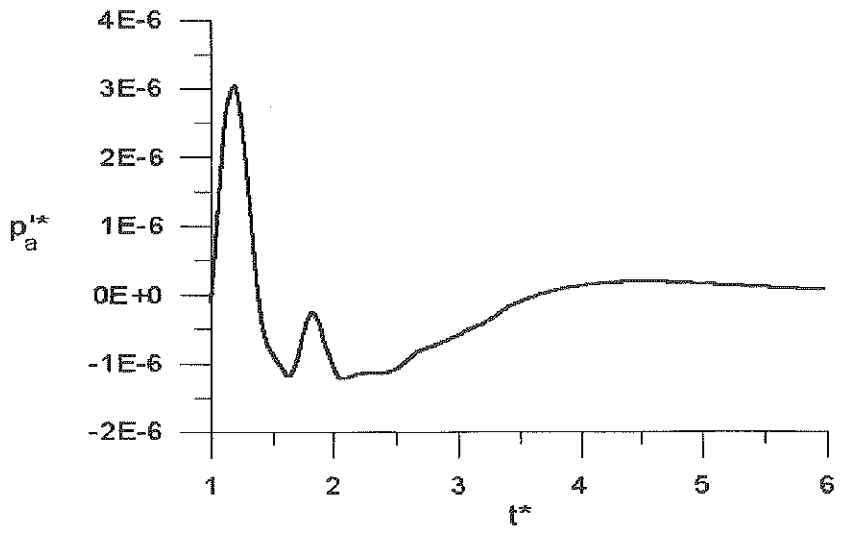

Fig. 6. Fluctuating acoustic pressure calculated from the decaying DNS of Fig. 4 ($p'^*_a = p'_a/(\rho_0 u'^2_0)$).

analysis of nonstationary signals, such as Figs. 5 and 6, is meaningful, we found that the peak frequency of the sound is roughly 2–4 times larger than the initial inverse eddy turnover time $\tau_{L_0}^{-1}$. A more complete analysis of frequency characteristics of the sound is given in Sec. 4.

The intensity of acoustic pressure is defined as

$$I = \frac{\langle (p'_a)^2 \rangle}{\rho_0 c_0}, \tag{3.5}$$

where $\langle \cdots \rangle$ implies ensemble average. In isotropic turbulence I depends only on the distance from the volume of turbulence x, and the acoustic power per unit mass is given by:

$$P = \frac{4\pi x^2}{\rho_0 V} I. \tag{3.6}$$

Proudman[2] showed from dimensional analysis that P is proportional to $M^5 u'^3/L$ and he predicted theoretically the coefficient of proportionality $\alpha = P/(M^5 u'^3/L)$. In Fig. 7 we plot the ensemble average of α as a function of time for the LES and DNS calculations. In these decaying simulations $\langle \alpha \rangle$ varied between 1.5 and 4, with average and standard deviation over $t^* \in [1, 6]$ of 2.5 ± 0.62 for the LES and 2.2 ± 0.99 for the DNS. In logarithmic scale the variations of α during time correspond to maximum ± 2 dB, which is reasonably low. Hence, we can conclude that the dimensional law predicted by Proudman is well satisfied.

The Proudman coefficients obtained with the two simulations are in good agreement and are also consistent with numerical results obtained by Sarkar and Hussaini,[8] who calculated $\alpha = 2.6$ with a decaying 64^3 DNS with initial $R_\lambda = 29$. The acoustic power generated by

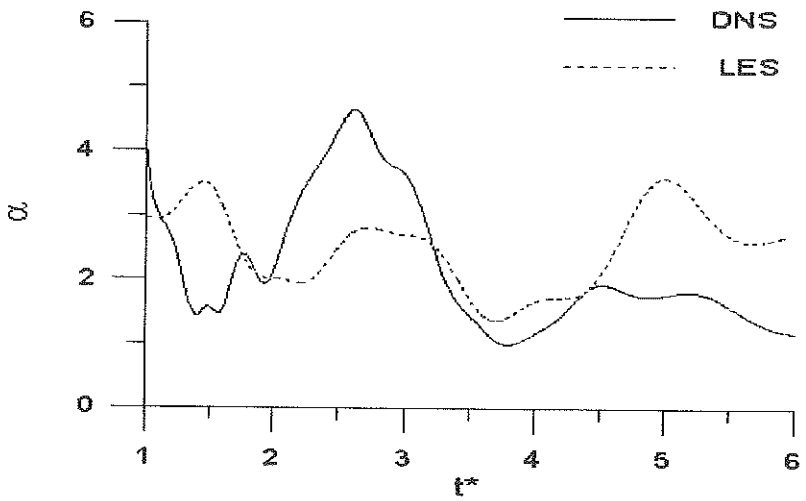

Fig. 7. Ensemble average of the Proudman coefficient α for the decaying turbulence simulations (LES and DNS).

the turbulence does not seem to depend critically on the Reynolds number of the isotropic turbulence or the type of simulation.

3.3. *Comparison with stochastic models*

There is no experimental data of noise generation by isotropic turbulence. However, the numerical results can be compared with two related theories for noise generation by isotropic turbulence developed by Proudman[2] and Lilley.[3] Both theories are based on Lighthill's equation (2.3) for far-field acoustic pressure. Proudman shows that, because acoustic pressure is given by the integral of second time derivatives of square velocity, acoustic intensity is given by the integral of a fourth-order correlation of velocity time derivatives within the turbulence at two points in space and in time. For homogeneous and isotropic turbulence (but not necessarily stationary) the correlation is a function only of space separation $r = \mathbf{y}' - \mathbf{y}$ and time separation $\tau = \frac{\mathbf{x}\cdot\mathbf{r}}{xc_0}$:

$$U(r,\tau,t) = \left\langle \left[\frac{\partial^2}{\partial t^2}(u_x^2 - \langle u_x^2\rangle)\right]_{\mathbf{y},t} \left[\frac{\partial^2}{\partial t^2}(u_x^2 - \langle u_x^2\rangle)\right]_{\mathbf{y}+\mathbf{r},t+\tau} \right\rangle \tag{3.7}$$

where $\langle\cdots\rangle$ implies ensemble average. Quantities in the first square bracket are evaluated at the point $\mathbf{y}$ at time t and quantities in the second square bracket are evaluated at the point $\mathbf{y}+\mathbf{r}$ at time $t+\tau$. The critical issue in both theories is to express the fourth-order correlation U as a function of simpler quantities which can be computed.

In developing his theory Proudman neglects time delay in the correlation U and assumes that the velocity and its first two time derivatives at two points in space have a normal joint probability distribution, so that fourth-order moments can be written as products of second-order moments. Using these two hypotheses, the fluid-motion equations and the properties

of homogeneous and isotropic turbulence, Proudman writes the coefficient α as a function of the longitudinal correlation function $f(\chi = r/L)$ and its derivatives. From the initial energy spectra of our LES and DNS decaying turbulence, we calculated the longitudinal correlation functions $f(\chi)$ at $t^* = 0$. Proudman's theory then gives $\alpha = 10$ for the LES and $\alpha = 13$ for the DNS. We checked that the value of α based on Proudman's model does not change significantly with time.

Lilley first assumes the turbulence to be quasi-stationary, reducing the correlation $U(r, \tau, t)$ to

$$U(r, \tau) = \frac{\partial^4}{\partial \tau^4} \langle [u_x^2]_{\mathbf{y},t} [u_x^2]_{\mathbf{y}+\mathbf{r},t+\tau} - \langle u_x^2 \rangle^2 \rangle \,. \tag{3.8}$$

He then assumes a normal joint probability distribution for velocity and, after several transformations, derives a relationship between α and the two-point two-time correlation $f(\chi, \tau)$. Finally, Lilley assumes independence of time and space variations of f:

$$f(\chi, \tau) = f_1(\chi) f_2(\Omega\tau) \,, \tag{3.9}$$

where Ω is the characteristic frequency of velocity fluctuations. The independence is somewhat artificial given that length and time scales are correlated in equilibrium turbulence. To predict α Lilley chooses $f_1(\chi)$ to be Gaussian and $f_2(\Omega\tau)$ to be consistent with the acoustic spectrum measured numerically in the isotropic decay DNS of Sarkar and Hussaini.[8] By separating $f(\chi, \tau)$, as in (3.9), Lilley shows that α depends on the turbulent Strouhal number $S_T = \Omega L/u'$ and on the flatness of velocity fluctuations T through the equation

$$\alpha = 1.8(T - 1) S_T^4 \,. \tag{3.10}$$

The typical value of T in isotropic turbulence is 3, but we do not know precisely the value of the Strouhal number for the decaying isotropic turbulence. If we suppose, after Lilley, that $S_T = 1$, we get $\alpha = 3.6$, which appears to be an improvement over Proudman's prediction of our numerically measured α. However, α predicted by (3.10) is very sensitive to S_T and if S_T is chosen to fit the form of Lilley's analytical acoustic spectrum to Sarkar and Hussaini's numerical spectrum, then $S_T = 1.24$ and (3.10) yields $\alpha = 8.5$

3.4. *Summary*

In summary, existing LES and low-Reynolds number DNS simulations predict the Proudman's constant in the range $\approx$ 2.2–2.6, whereas Proudman's theory gives $\alpha \approx$ 10–13. The difference between the numerical calculation and Proudman's prediction may be due to the hypothesis of quasi-normality employed by Proudman for velocity and its first two time derivatives. Lilley theory yields $\alpha = 3.6$ assuming $S_T = 1$, but $\alpha = 8.5$ with $S_T = 1.24$, based on numerical results obtained by Sarkar and Hussaini. A difficulty with the Lilley theory is that it yields a prediction for α very sensitive to the Strouhal number, which is not known with precision. The sound spectra indicate that the characteristic frequency of the generated noise is greater than the characteristic frequency of the large eddies $\omega_L = u'/L$.

4. Sound Generation by Stationary Isotropic Turbulence

Because the absence of turbulence production leads to rapid changes in turbulence characteristics, in this section we study the noise generated by stationary isotropic turbulence using 128^3 forced DNS. Using this higher resolution DNS, we also analyze relative contributions of different turbulent scales to noise generation, an important issue which cannot be studied with decaying isotropic turbulence.

4.1. *Turbulence simulation*

Stationary isotropic turbulence was obtained using the pseudo-spectral algorithm designed for the massively parallel connection machine by Chen and Shan.[16] To have the widest possible range of turbulence length scales (within practical limits) with all scales well resolved, we developed stationary turbulence at low Reynolds number ($R_\lambda = 20$) on a 128^3 grid. The characteristics of the stationary state are given in the last column of Table 1.

To create stationary turbulence, energy must be added to the flow at the rate lost by dissipation. This is done by forcing the Navier–Stokes equations such that, at each time step, the rate of energy added by forcing balances the rate of energy lost through friction. Whereas a number of different forcing schemes may be found in the literature, none is useful to our study where it is important that the turbulence contain realistic integral as well as dissipation-scale eddies. Consequently, we developed our own forcing algorithm.

The first requirement of our forcing scheme is to maintain fixed energy and dissipation-rate spectra close to spectra of fully-developed decaying isotropic turbulence, in a manner which does the least damage to the turbulence structure so that the relative contributions to the generation of noise may be studied. Secondly, the forcing scheme must ensure the continuity of second time derivatives of velocity, which is fundamental to acoustic computations using Eq. (2.3). To this end we add proportionally the energy lost by dissipation during each time step to a wide range of large-scale modes, as illustrated in Fig. 8, without altering the phases of the forced Fourier modes.

More specifically, after advancing in time by one time step Δt each Fourier coefficient $\hat{\mathbf{u}}(\mathbf{k}, t + \Delta t)$ of modes in the range $[k_{\min}, k_{\max}]$ is multiplied by a scalar β, which depends on the ratio of energy lost by dissipation during the time step (ΔE_{tot}) to the total energy contained in the band $[k_{\min}, k_{\max}]$:

$$\hat{\mathbf{u}}(\mathbf{k}, t + \Delta t) = \beta \hat{\mathbf{u}}(\mathbf{k}, \Delta t) \quad \text{for } k \in [k_{\min}, k_{\max}], \tag{4.11}$$

where

$$\beta = \sqrt{1 + \frac{\Delta E_{\text{tot}}}{\int_{k_{\min}}^{k_{\max}} E(k) dk}}. \tag{4.12}$$

After some numerical experimentation we chose $[k_{\min}, k_{\max}] = [3, 20]$.

Stationarity was achieved after forcing for about $3\tau_L$. The nearly stationary energy and dissipation spectra at time $15\tau_L$ after initiating forcing are shown in Fig. 9 (the total simulation time is $30\tau_L$). These are close to the spectra obtained for fully-developed

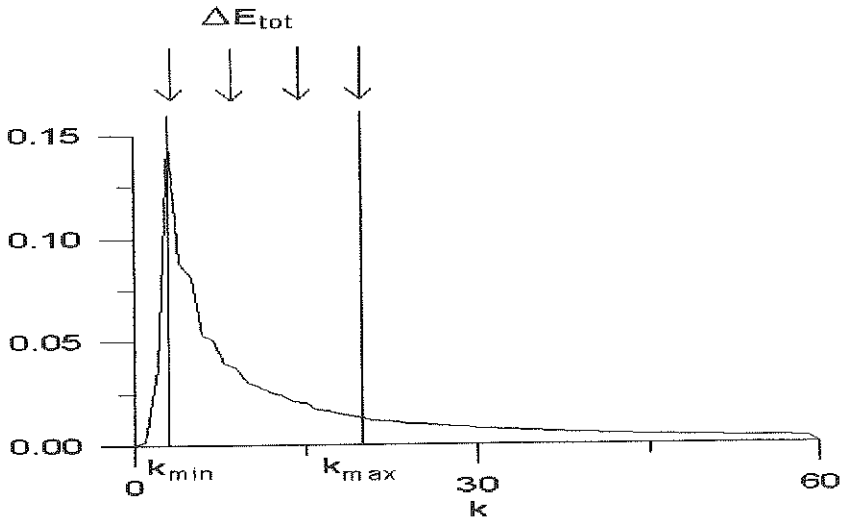

Fig. 8. Initial energy spectrum and the range $[k_{\min}, k_{\max}]$ of Fourier modes over which the forcing is applied. The spectrum is shown normalized by total energy.

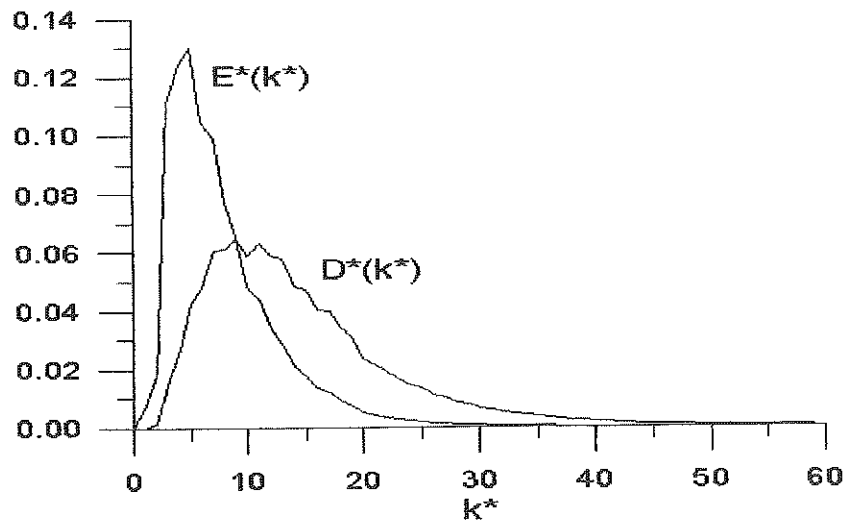

Fig. 9. Energy and Dissipation spectra at $t = 15\tau_L$ (normalized by total energy and dissipation-rate, respectively).

decaying isotropic turbulence with a similar simulation.[17] Similarly, the integral length scale, Taylor microscale, dissipation rate, velocity derivative skewness and flatness are close to those obtained from decaying isotropic turbulence simulation. Also, visualizations of 3D isosurfaces of energy and enstrophy show qualitatively the same structure as that in Yeung and Brasseur's simulation.

We conclude that the forced simulations provide instantaneous velocity fields of isotropic stationary turbulence with realistic energy-scale and dissipation-scale structure. Eight realizations of stationary isotropic turbulence were simulated for about $30\tau_L$.

From the time-varying velocity field the instantaneous acoustic pressure far from the turbulence volume is computed using the form of Lighthill's analogy given by Eq. (2.3).

4.2. *Acoustics computations*

4.2.1. *Acoustic pressure*

The acoustic pressure was computed with expression (2.3) at a distance $x = 20D$ from the center of the turbulence box for the 8 realizations. The acoustic pressure obtained for a typical realization is shown in Fig. 10, indicating approximate stationarity.

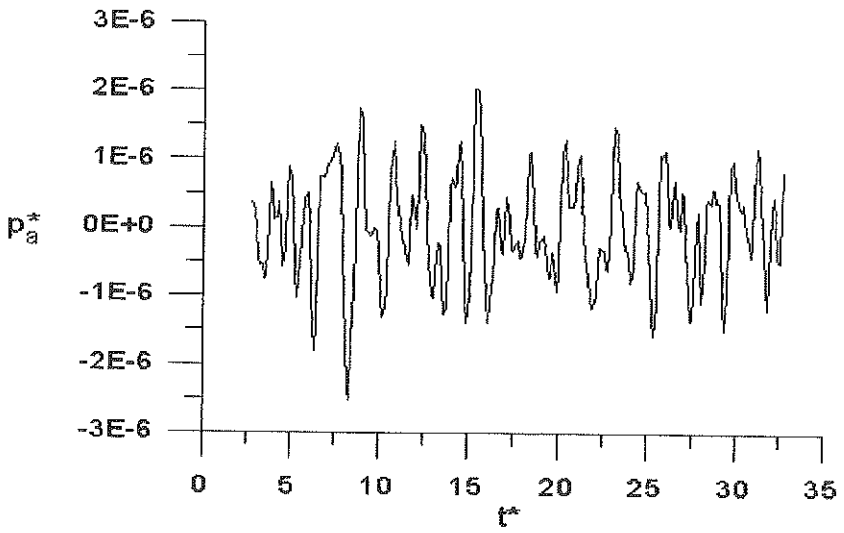

Fig. 10. Acoustic pressure ($t^* = t/\tau_L$, $p_a^* = p_a/(\rho_0 c_0^2)$).

4.2.2. *Acoustic power*

The intensity of a stationary acoustic signal is given by

$$I = \frac{\overline{(p_a - \overline{p}_a)^2}}{\rho_0 c_0}, \tag{4.13}$$

where the overbar implies time average. The acoustic power per unit mass of isotropic turbulence is given by Eq. (3.6). Acoustic intensity, acoustic power and the Proudman constant α were calculated for each realization and averaged.

We find that the mean value of α computed over 8 independent realizations is 2.1, consistent with numerical results obtained previously for decaying isotropic turbulence, both by ourselves ($\alpha = 2.1$ with a decaying DNS and $\alpha = 2.6$ with a decaying LES) and

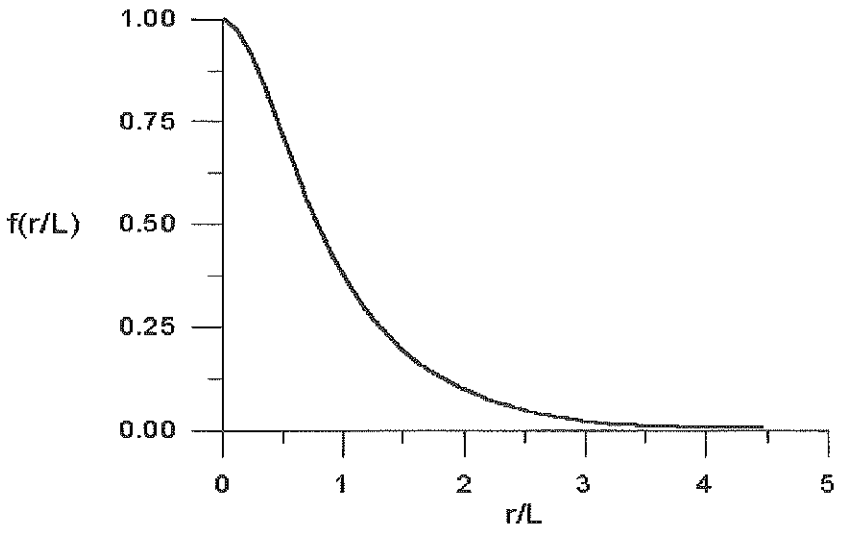

Fig. 11. Longitudinal correlation function $f(r)$ computed from DNS.

Sarkar and Hussaini ($\alpha = 2.6$ with a decaying DNS).[8] Hence, forcing does not seem to alter the global acoustic power generated by turbulence.

To compare our results with Proudman's model, we computed the correlation function $f(\chi)$ for the forced DNS (Fig. 11). Using the numerical form of $f(\chi)$ and Proudman's expression for α, we obtain $\alpha = 14$. Hence, the difference between the computed value of α and the value given by Proudman's model is close to that obtained with decaying isotropic turbulence.

In order to compare our results to Lilley's model we attempted to use the numerical forms of $f_1(\chi)$ and $f_2(\tau)$ [Eq. (3.9)]. However, the prediction of α is very sensitive to $f_2(\tau)$, making it difficult to obtain α with precision from the numerically computed form of $f_2(\tau)$. To estimate α from Lilley's theory, we therefore used the analytical expression proposed by Lilley for $f_2(\tau)$ and the numerical result of Fig. 11 for $f_1(\chi)$ to obtain:

$$\alpha = 1.4(T-1)S_T^4 . \tag{4.14}$$

If we take $S_T = 1$, α equals 2.8. If we fit the peak of Lilley's analytical acoustic spectrum to the peak of our DNS numerical acoustic spectrum, we obtain $S_T = 1.4$ and $\alpha = 10.8$.

4.2.3. *Acoustic pressure spectrum*

Because the acoustic pressure is stationary, it is appropriate to compute the acoustic frequency spectrum of the far-field sound as the Fourier transform of the acoustic pressure. The spectrum shown in Fig. 12 is the average over 8 realizations.

We find that the spectrum peaks at an angular frequency four times the inverse eddy turnover time. To compare the peak frequency of pressure fluctuations with the peak frequency of velocity fluctuations, we computed the ensemble averaged spectrum of

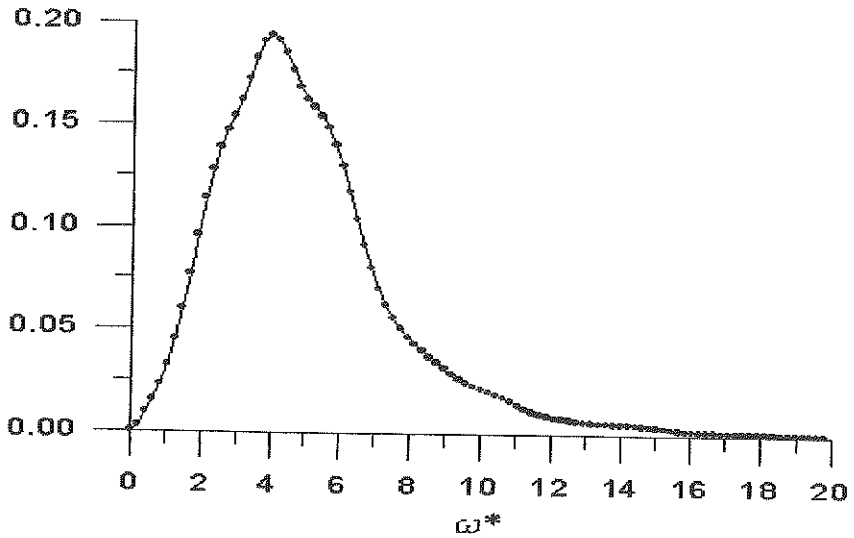

Fig. 12. Acoustic pressure spectrum averaged over 8 realizations and normalized by the total acoustic power ($\omega^* = \omega L/u'$).

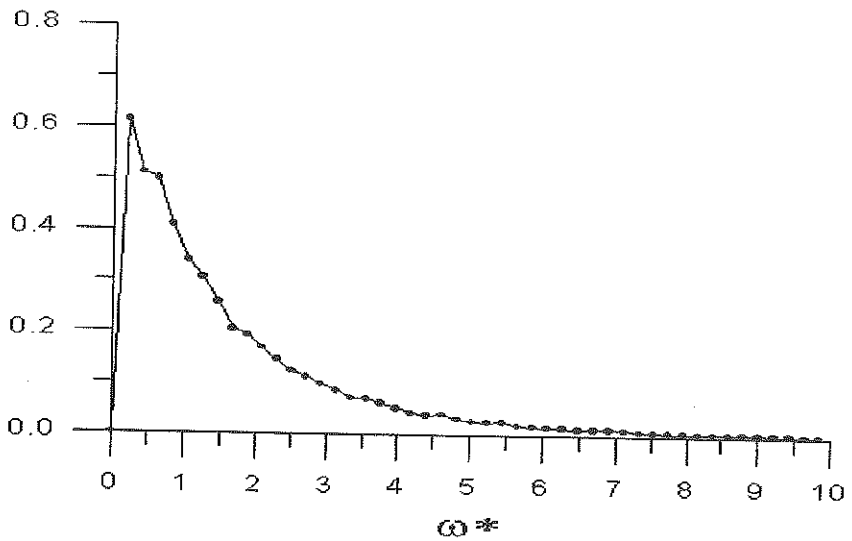

Fig. 13. Velocity fluctuations spectrum averaged over 8 realizations and normalized by the total energy ($\omega^* = \omega L/u'$).

temporal velocity fluctuations for 30 points in the turbulence volume and for 8 realizations. We find that the acoustic pressure spectrum peaks at a frequency approximately 12 times higher than the turbulent velocity spectrum (Fig. 13), suggesting that turbulence scales below the integral scale contribute significantly to noise generation from isotropic turbulence.

4.3. *Relative contributions of turbulence scales to noise generation*

It is typically assumed that integral-scale motions are primarily responsible for the radiated noise for fully developed turbulence. Figures 12 and 13, however, suggest a potentially significant role for scales below the integral scale. However, the relationship between frequency and wavenumber spectra in turbulence is not clear.

In this section we attempt to quantify contributions from different turbulence scales to the noise by filtering the velocity field in Fourier space and computing separately the acoustic power generated by the filtered fields. For this purpose we used low-pass and high-pass filters with variable filter cut-off k_c. From the filtered velocity fields we computed separately the fluctuating acoustic pressure $p_a^l(\mathbf{x}, t)$ generated by "larger" scales ($k < k_c$) and the fluctuating acoustic pressure $p_a^s(\mathbf{x}, t)$ generated by "smaller" scales ($k > k_c$). The total acoustic pressure p_a^{tot} generated by the entire velocity field is given by

$$p_a^{\text{tot}} = p_a^s + p_a^l + 2p_a^{sl}\,, \tag{4.15}$$

where the cross-correlation contribution is

$$p_a^{sl}(\mathbf{x}, t) = \frac{\rho_0}{4\pi c_0^2}\frac{1}{x}\int_V \left[\frac{\partial^2 u_x^s u_x^l}{\partial t^2}\right] dV\,. \tag{4.16}$$

Because Fourier modes across a hard filter cut-off are statistically uncorrelated, and (4.16) is equivalent to a spatial mean (the effect of time delay is minimal) p_a^{sl} is negligible compared to p_a^s and p_a^l and

$$p_a^{\text{tot}} \simeq p_a^s + p_a^l\,. \tag{4.17}$$

We have numerically verified this conclusion. From the acoustic pressure we deduce the intensity I^l due to the "larger" scales, the intensity I^s due to the "smaller" scales and the cross intensity I^{sl} due to the correlation between smaller and larger scales

$$I^{sl} = \frac{\overline{p^s p^l}}{\rho_0 c_0} \tag{4.18}$$

where

$$I^{\text{tot}} = I^s + I^l + 2I^{sl}\,. \tag{4.19}$$

This time the correlation I^{sl} is a time mean. Although "smaller" and "larger" scales are separated in Fourier space by a hard filter cut-off, they are not necessarily well separated in frequency space, which means that two different scales can generate sound of the same frequency. Consequently, the correlation I^{sl} is not necessarily small. As illustrated in Fig. 14 we chose different cut-off wavenumbers k_c focusing on the region between energy and dissipation spectra peaks. In Fig. 15 we compare energy carried by "larger" scales ($k < k_c$) with dissipation carried by "smaller" scales ($k < k_c$) as a function of k_c. Note that there are equal amounts of energy and dissipation (about 70%) on either side of the cut-off when $k_c = 9$. Because the dissipation-rate and enstrophy spectra are the same in

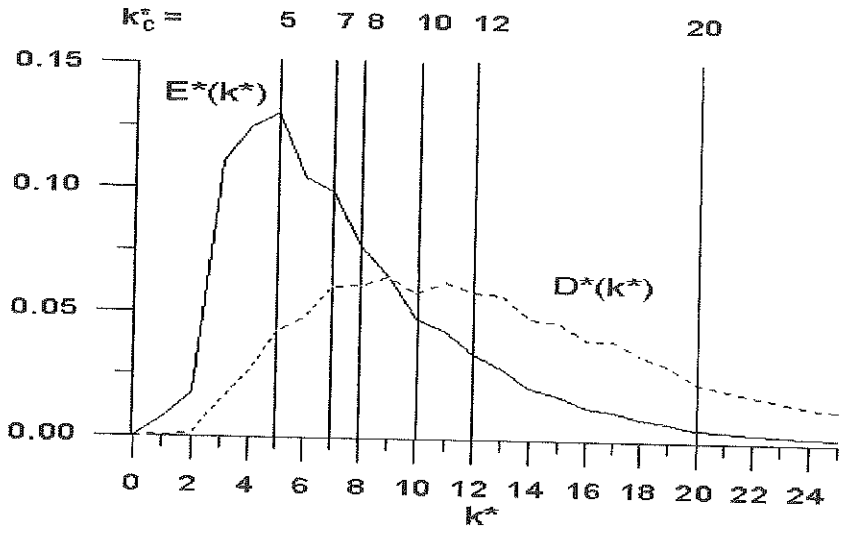

Fig. 14. The cut-off wavenumber compared with energy and dissipation spectra ($t = 15\tau_L$).

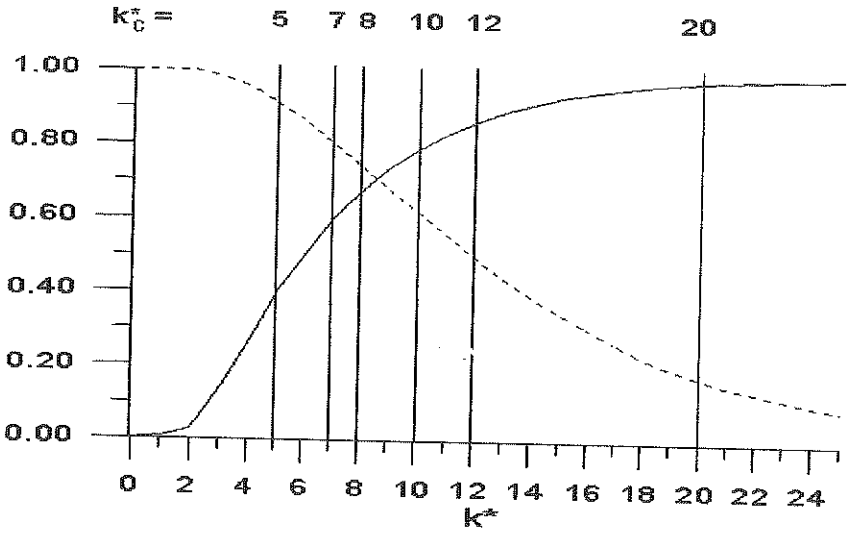

Fig. 15. Energy carried by "larger" scales $\int_0^k E(k)dk$ (in solid line) and dissipation carried by "smaller" scales $\int_k^\infty D(k)dk$ (in dashed line) compared with the cut-off k_c.

homogeneous turbulence, the same statement can be made about the relative content of energy and entrophy when $k_c = 9$.

For every value of k_c 3 to 5 realizations were calculated for $30\tau_L$ and the acoustic intensity was computed as an ensemble average over the realizations. The relative acoustic intensities generated by "smaller" eddies (I^s), by "larger" eddies (I^l) and the cross intensity (I^{sl}) are shown in Fig. 16 as functions of the filter cut-off wavenumber.

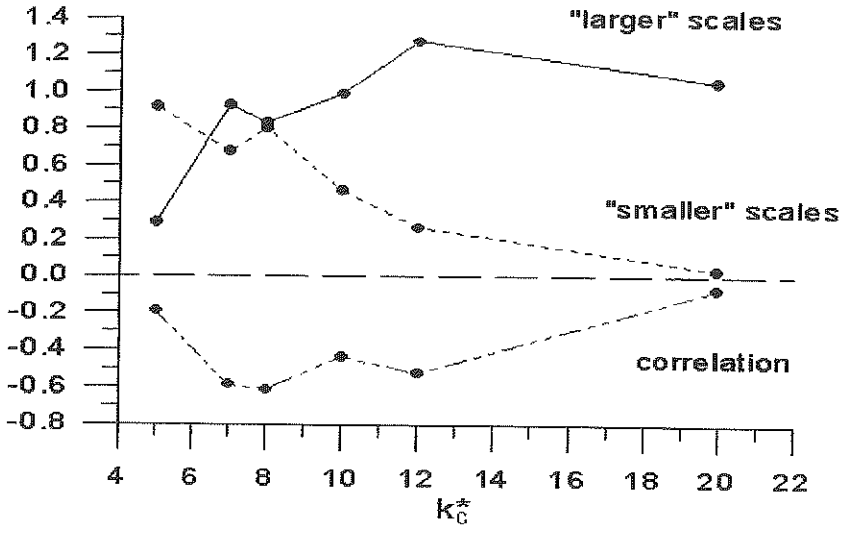

Fig. 16. Relative intensities: I^s/I^{tot}, I^l/I^{tot} and I^{sl}/I^{tot}.

From the plot we may draw several conclusions.

Firstly, we observe that the contributions to the far-field noise from wavenumbers smaller than 5 and wavenumbers larger than 12 are negligible. Secondly, most of the radiated noise comes from wavenumbers roughly between 6 and 10, between the peaks of the energy and dissipation spectra (see Fig. 14). These scales carry significant levels of both energy and dissipation (see Fig. 15). Thirdly, the contribution to I^{tot} from the correlation between acoustic pressure generated by "smaller" scales and "larger" scales is large, especially for the scales primarily responsible for noise generation ($k \in [6, 10]$), suggesting that the scales corresponding to wavenumbers on both sides of the cut-off k_c can generate sound at the same frequency.

We conclude that the primarily scales responsible for noise generation lie between energy and dissipation-range scales. In the current simulation the primary noise sources are at scales 2–3 times smaller than the energy-containing scales and 1.5–2 times larger than the dissipation/vorticity dominated scales. However, because the Reynolds number of the simulated turbulence is low, the peaks in the energy and dissipation spectra are not well separated and there is no inertial range. Consequently, it is difficult to know if the intermediate scales in the simulation generate noise because they still carry a significant amount of energy, or because they carry a high level of the vorticity or dissipation. Likely both are true.

This calculation is also relevant to the use of LES in acoustic noise computations. The results of Fig. 16 suggest that a LES must include scales at least 2–3 times smaller than the integral length scale in order to capture the most productive acoustic sources. It is possible, therefore, that the decaying LES described in Sec. 2 has an insufficient spatial resolution.

However, because the energy spectra of the DNS and the LES are very different it is difficult to draw categorical conclusions.

5. Conclusions

The simulations described herein suggest that acoustic power generated by isotropic turbulence is proportional to $M^5 u'^3/L$, with the coefficient of proportionality α slightly larger than 2 ($\alpha = 2.2$ with decaying DNS, 2.5 with decaying LES and $\alpha = 2.1$ with forced DNS). Our stationary, high-resolution DNS indicates that the acoustic pressure spectrum (Fig. 12) peaks at a frequency four times higher than the inverse eddy turnover time and over a decade higher than the peak in the velocity frequency spectrum, suggesting that the dominant acoustic sources are within eddies smaller that the integral-scale. Spectral filtering of the simulated velocity field indicates that, for the studied low Reynolds number turbulence, the turbulence scales primarily responsible for the generated noise lie between the energy and vorticity dominant scales.

Acknowledgments

The computations were performed with computer time provided by the Pittsburgh Supercomputing Center, Nasa Ames Research Center and IDRIS (Institut du Développement et des Ressources en Informatique Scientifique). The LES code was kindly provided by J. P. Bertoglio of Ecole Centrale de Lyon. The PSC computations were carried out using a parallelized pseudo-spectral code kindly provided by Sh. Chen of the Watson Research Laboratory at IBM. We thank J. P. Bertoglio, W. Shao, S. Sitharaman and L. P. Wang for their help in developing and running the codes.

Alicja Witkowska gratefully acknowledges financial support from the Office of International Programs and the College of Engineering at Pennsylvania State University.

References

1. M. J. Lighthill, "On sound generated aerodynamically," *Proc. Roy. Soc. London* **1** (1952) 564–587.
2. I. Proudman, "The generation of noise by isotropic turbulence," *Proc. Roy. Soc. London* **A214** (1952), 119–132.
3. M. J. Lilley, "The radiated noise from isotropic turbulence revisited," *ICASE Technical Report 93-75* (1993).
4. T. Colonius, S. K. Lele and P. Moin, "Direct computation of the sound generated by a two-dimensional shear layer," *AIAA Paper 93-4328* (1993).
5. B. E. Mitchell, S. K. Lele and P. Moin, "Computations of the far-field sound radiated by an axisymmetric jet," in *Flow Acoustics: A Technology Audit* (Ecole Centrale de Lyon, 1994), pp. 13–16.
6. W. Béchara, "Modélisation du bruit d'écoulements turbulents libres," Ph.D. thesis, Ecole Centrale de Paris, N 92-02 (1992).
7. C. Bailly, P. Lafon and S. Candel, "Stochastic approach to noise modelling for free turbulent flows," in *Flow Acoustics: A Technology Audit* (Ecole Centrale de Lyon, 1994).
8. S. Sarkar and M. Y. Hussaini, "Computation of the sound generated by isotropic turbulence," *ICASE Technical Report 93-74* (1993).

9. S. C. Crow, "Aerodynamic sound emission as a singular perturbation problem," *Stud. Appl. Math.* **49**(1) (1970), 21–44.
10. A. Witkowska and D. Juvé, "Estimation numérique du bruit rayonné par une turbulence homogène et isotrope," *C. R. Acad. Sci. Paris t. 318* (Série II) (1994), 597–602.
11. A. Powell, "The theory of vortex sound," *J. Acoust. Soc. Am.* **36** (1964), 177–195.
12. J. C. Hardin, "Noise calculation on the basis of vortex flow models," in *ASME Symposium on Noise and Fluid Engineering*, Atlanta, GA, 1977.
13. W. Möhring, "On vortex sound at low mach number," *J. Fluid. Mech.* **85**(4) (1978), 685–691.
14. J. P. Chollet and M. Lesieur, "Parametrization of small scales of three-dimensional isotropic turbulence utilizing spectral closures," *J. Atm. Sci.* **38** (1981), 2747–2757.
15. A. Witkowska, "Estimation numérique du bruit rayonné par une turbulence isotrope," Ph.D. thesis, École Centrale de Lyon, N 94-58 (1994).
16. S. Chen and X. Shan, "High-resolution turbulent simulations using the connection machine-2," *Computers in Physics* **6**(6) (1994), 643–646.
17. P. K. Yeung and J. G. Brasseur, "The response of isotropic turbulence to isotropic and anisotropic forcing at the large scales," *Phys. Fluids* **A3** (1991), 884–897.